







Article

Engineering Ligament Scaffolds Based on PLA/Graphite Nanoplatelet Composites by 3D Printing or Braiding

Magda Silva ^{1,2,3}, Isabel Pinho ³, Hugo Gonçalves ³, Ana C. Vale ^{1,2} , Maria C. Paiva ³ , Natália M. Alves ^{1,2,*} 
and José A. Covas ^{3,*} 

¹ 3B's Research Group, I3Bs—Research Institute on Biomaterials, Biodegradables and Biomimetics, University of Minho, Headquarters of the European Institute of Excellence on Tissue Engineering and Regenerative Medicine, Avepark, 4805-017 Guimarães, Portugal

² ICVS/3B's, Associate PT Government Laboratory, 4710-057 Braga/4805-017 Guimarães, Portugal

³ Department of Polymer Engineering, Institute for Polymers and Composites, University of Minho, 4800-058 Guimarães, Portugal

* Correspondence: nalves@i3bs.uminho.pt (N.M.A.); jcovas@dep.uminho.pt (J.A.C.)

Abstract: The development of scaffolds for tissue-engineered growth of the anterior cruciate ligament (ACL) is a promising approach to overcome the limitations of current solutions. This work proposes novel biodegradable and biocompatible scaffolds matching the mechanical characteristics of the native human ligament. Poly(L-lactic acid) (PLA) scaffolds reinforced with graphite nano-platelets (PLA+EG) as received, chemically functionalized (PLA+f-EG), or functionalized and decorated with silver nanoparticles [PLA+((f-EG)+Ag)], were fabricated by conventional braiding and using 3D-printing technology. The dimensions of both braided and 3D-printed scaffolds were finely controlled. The results showed that the scaffolds exhibited high porosity (>60%), pore interconnectivity, and pore size suitable for ligament tissue ingrowth, with no relevant differences between PLA and composite scaffolds. The wet state dynamic mechanical analysis at 37 °C revealed an increase in the storage modulus of the composite constructs, compared to neat PLA scaffolds. Either braided or 3D-printed scaffolds presented storage modulus values similar to those found in soft tissues. The tailorable design of the braided structures, as well as the reproducibility, the high speed, and the simplicity of 3D-printing allowed to obtain two different scaffolds suitable for ligament tissue engineering.

Keywords: ligaments; 3D-printed scaffold; textile-engineered scaffold; functionalized graphene; PLA; composites



Citation: Silva, M.; Pinho, I.; Gonçalves, H.; Vale, A.C.; Paiva, M.C.; Alves, N.M.; Covas, J.A. Engineering Ligament Scaffolds Based on PLA/Graphite Nanoplatelet Composites by 3D Printing or Braiding. *J. Compos. Sci.* **2023**, *7*, 104. <https://doi.org/10.3390/jcs7030104>

Academic Editor: Francesco Tornabene

Received: 24 December 2022

Revised: 22 February 2023

Accepted: 3 March 2023

Published: 7 March 2023



Copyright: © 2023 by the authors. Licensee MDPI, Basel, Switzerland. This article is an open access article distributed under the terms and conditions of the Creative Commons Attribution (CC BY) license (<https://creativecommons.org/licenses/by/4.0/>).

1. Introduction

Scaffold engineering for ligament tissue regeneration is a promising strategy to heal ligaments with severe injuries, overcoming the inadequacies of current treatments involving auto and allografts [1]. The approach consists in incorporating specific cells into a compatible scaffold to be implanted into the lesion site, with combined cell growth and scaffold degradation. Providing the required scaffold morphology and mechanical performance, as well as using the adequate scaffold material and cell type, enables the formation of a new tissue that replaces the damaged one, restoring its functionality [2,3].

The scaffold properties, such as biocompatibility, biodegradability, and mechanical performance, are directly influenced by the composition of the material used [4]. Many biomaterials have been evaluated for ligament TE, including natural materials (e.g., collagen; silk), biodegradable synthetic polymers (e.g., poly(L-lactic acid) (PLA), poly(glycolic acid) (PLGA)), and composites/blends (e.g., PLA-collagen, polycaprolactone-collagen, and PLA-PLGA) [5]. Among synthetic polymers, formulations based on PLA scaffolds have been widely developed [6–8], presenting superior mechanical properties and fibroblast proliferation when compared to other biodegradable polymers such as polyglycolic acid [7].

PLA is a biodegradable and biocompatible polymer produced from renewable bio-based resources such as corn or cellulose [4]. The median half-life of the polymer is 30 weeks and produces safe hydrolytic degradation products (lactic acid or carbon dioxide and water), naturally metabolized by the human body through the kidneys or breath. PLA-based materials have been routinely used for several medical applications such as drug delivery, TE implants, or sutures [9].

Graphene-based materials such as carbon nanotubes (CNTs) and graphene nanoplatelets (GNPs) exhibit unique properties and have been effective as fillers for polymer reinforcement [10], resulting in composites with superior mechanical, thermal, and electrical properties [11,12]. Gonçalves et al. [10] incorporated graphene nanoplatelets in PLA at different loadings (0.1–0.5 wt.%) and observed that the composite with 0.25 wt.% filler presented a 20% increase in tensile strength and a 12% increase in the Young's modulus. Novais et al. showed that the functionalization of graphite nanoparticles through a 1,3-dipolar cycloaddition (DCA) of an azomethine ylide improved the composite interfacial strength, through covalent bonding of PLA with the pyrrolidine group formed at the graphene surface [13,14]. Moreover, the morphology and metabolic activity of human fibroblasts (HFF-1) were not affected by the presence of graphene [10]. The combination of graphene and its derivatives with biocompatible polymeric matrices is also attractive for TE scaffolds because of their high surface area and nanoscale dimension that matches the size of cell surface receptors, and the natural extracellular matrix (ECM) nanotopography [15,16]. Composite scaffolds with low graphene or functionalized graphene content have been considered to reduce the potential cytotoxicity in the human body [15,16].

An important concern during the implantation of a scaffold is the risk of bacterial infections at implant or device sites, which are frequently difficult to treat due to deep tissue localization and the bacteria involved [17]. The incorporation of antibacterial components into scaffolds may aid appropriate postoperative regeneration of the scaffold implantation site [18]. Silver nanoparticles have demonstrated interesting activity in tissue regeneration because of their nano-size, high inherent antimicrobial efficiency, and capacity to accelerate the healing process and production of ECM components [19,20]. To facilitate recovery after ACL-reconstructive surgery, the use of electrical stimulation has been recommended [3,21,22]. As a metallic agent, silver nanoparticles can also change the electrical characteristics of the cells [23]. The combination of polymers with metallic nanoparticles, e.g., silver nanoparticles, and carbon fillers, is thus an attractive way to enhance the transmission of an electrical stimulation applied from skin electrodes to the damaged tissue, enhancing its repair [3]. A decoration of functionalized graphene surfaces with silver nanoparticles can be easily obtained through a reaction based on the reduction of silver ions by *N,N*-dimethylformamide [24,25].

Current fabrication methods for ligament scaffolds include melt spinning, electrospinning, freeze-drying, solvent casting, hydrogel solution mixing, and additive manufacturing [26]. Fibrous scaffolds have been the preferred choice to mimic the hierarchical organization of native ligaments [27]. These structures are based on an assembly of fibers, either random or aligned in parallel, as a rope, or arranged by braiding [6,7], braid-twisting [8], or knitting [28], as typically performed in the textile industry [27,29].

Additive manufacturing (AM), also known as three-dimensional (3D) printing, has revolutionized the regenerative medicine field due to its capacity of producing customizable scaffolds for tissue engineering [30] with controlled pore size and structure [31]. AM enables the production layer by layer of complex and precise structures with high reproducibility [32]. Recently, scaffolds have been produced by bioprinting, stereolithography, inkjet printing, selective laser sintering [31], and fused deposition modeling (FDM) techniques. FDM is one of the most widespread, simple, and cheap 3D printing methods, whereby a continuous filament of a thermoplastic polymer is extruded through a nozzle and subsequently deposited onto a print bed, creating successive horizontal thin layers of the part in the vertical direction [18,30]. FDM does not require solvents and can use a

variety of biodegradable and biocompatible materials, the most common being PLA, to fabricate 3D printed scaffolds [4,18].

Previously, the authors reported the successful production of PLA/graphite nanoplatelet composite filaments with enhanced mechanical and electrical properties [24]. Here, those filaments are used to obtain scaffolds for ligament regeneration. Two alternative manufacturing techniques were investigated, one based on braiding, the other using FDM. Braided scaffolds benefit from the tailorable structures that may be obtained by conventional textile techniques to mimic the native ligament morphology. FDM is a simple, fast, and cost-effective technique that, to the best of our knowledge, has not yet been utilized to obtain scaffolds based on PLA/graphene composites for ACL. The present work reports the production, optimization, and characterization of these composite scaffolds based on PLA and graphite nanoplatelets (PLA+EG), functionalized EG (PLA+f-EG) and f-EG with a low concentration of silver nanoparticles anchored at the surface [PLA+((f-EG)+Ag)]. These scaffolds were produced with controlled architecture, adequate porosity, and mechanical properties relevant for the re-generation of the ACL.

2. Materials and Methods

2.1. Scaffolds Production

2.1.1. Materials

PLA filaments and PLA composite filaments with two different diameters (0.26 ± 0.03 mm, designated as FilText, and 1.71 ± 0.07 mm, designated as Fil3D), produced in a previous work [24], were used in the preparation of the textile engineered and 3D printed scaffolds, respectively. The composite filaments were constituted by PLA and EG at weight concentrations of 0.25, 0.5, 1, and 2 wt.%, as determined by thermogravimetric analysis on a TGA Q500 equipment (TA Instruments®, New Castle, DE, USA) at 800 °C, under a nitrogen atmosphere at a flow rate of 50 mL min⁻¹—Table S1 in Supplementary Material. The PLA was the grade Luminy LX175 from Total Corbion, Gorinchem, and the EG were Micrograf HC11 obtained from Nacional de Grafite Lda, Minas Gerais, Brasil. The EG were functionalized by the DCA reaction (f-EG), and (f-EG) were decorated with silver nanoparticles [(f-EG)+Ag], as previously described [24]. The melt flow index (MFI) of the filaments containing PLA and PLA reinforced with 0.5 and 2 wt.% of fillers was measured at 185 °C and a load of 2.16 kg on MFI equipment from Daventest (Welwyn Garden City, England).

2.1.2. Three-Dimensional Printing

The 3D-printed scaffolds were designed using the Ultimaker Cura (version 4.4, Ultimaker, Geldermalsen, Netherlands) software (Figure 1), with an infill linear pattern (0 and 90°) and porosity of 50%. The scaffold was printed horizontally using an Ender-3 3D Printer from Creality (London, UK).

2.1.3. Braiding

Braided scaffolds were manufactured using the FilText filaments reinforced with 0.5 and 1 wt.% of [(f-EG)+Ag]. The textile-engineered scaffolds made with FilText filaments were produced using a *kumihimo* hand braiding device, with a circular stand (diameter of 12 cm). The *kumihimo* technique and the resulting braided structure (formed by 8 FilText filaments and designated as bundle) are represented in Figure 2a,b, respectively.

The number of bundles was optimized to obtain a braided scaffold with a diameter of approximately 9 mm, similar to the native ligament. The resulting scaffold comprises an exterior braided structure formed by 8 FilText filaments and a core containing 8 bundles aligned in parallel and tied together with a suture of the same material (Figure 2c).

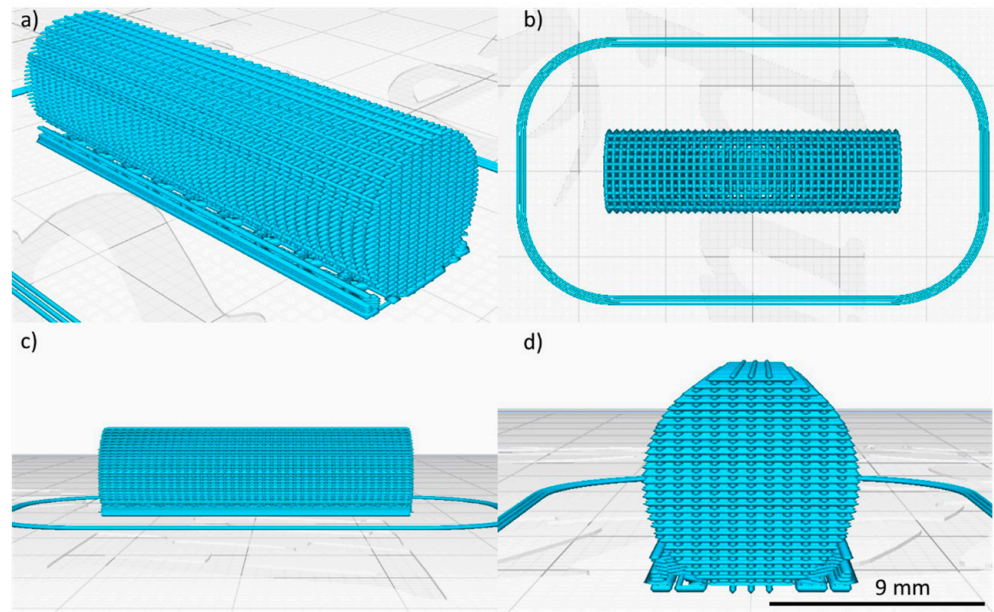


Figure 1. Three-dimensional-printed scaffolds. (a) Isometric view; (b) top view; (c) lateral view; and (d) front view.

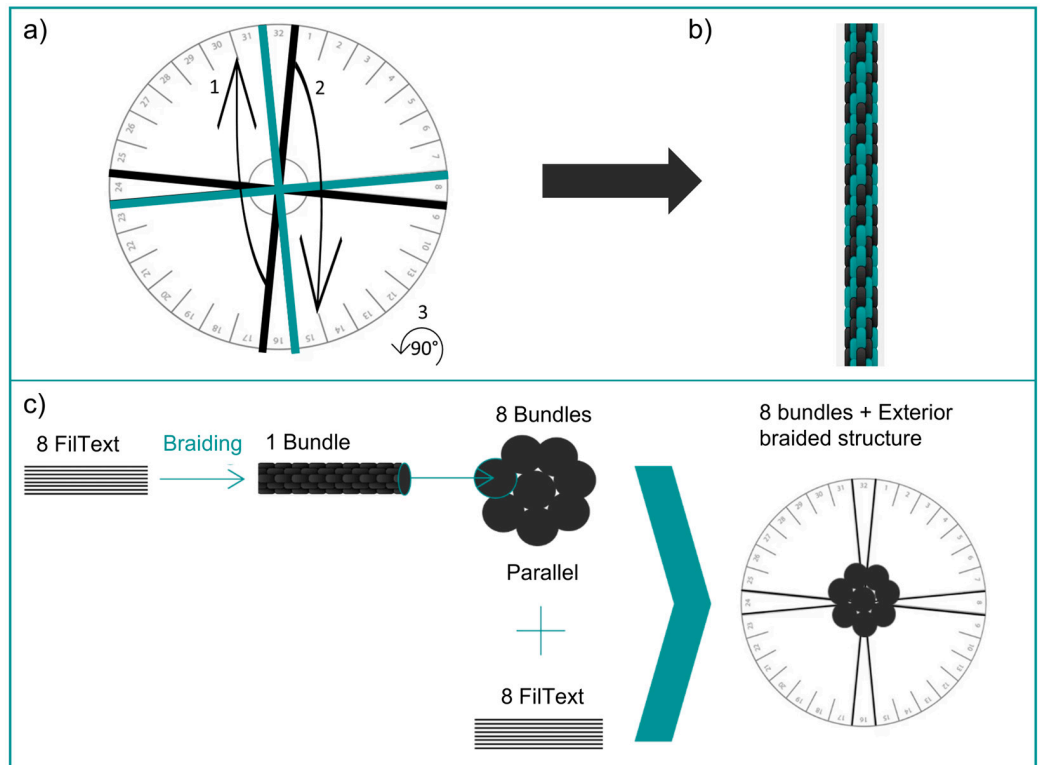


Figure 2. (a) *Kumihimo* technique: slot 32 of the disk is placed in the 12 o’clock position. Eight FilText filaments are tied together, placed in the center of the disk, and the loose ends loaded into slots 31 and 32, 7, and 8, 15 and 16, 23, and 24 on the *kumihimo* disk. Then, FilText filaments are moved from slot 16 to 30 (1) and 32 to 14 (2). Then, the disk is rotated 90° counterclockwise (3) and the FilText filaments moved from slot 24 to 6 and slot 8 to 22. This procedure was repeated until the required braid length was reached; (b) braided structure obtained after multiple repetitions of (a); (c) structure of the final braided scaffold.

2.2. Scaffold Characterization

Both types of scaffolds exhibited a cylindrical shape with a full length of approximately 32 mm and a diameter of 9 mm, which are comparable to the dimensions of the native ACL. Smaller braided and 3D-printed scaffolds with an approximate length of 25 mm and diameter of 4 mm were also produced for further testing.

The morphology and the shape, size, and distribution of the pores of braided and 3D-printed scaffolds were analyzed using a Digital Microscope Leica DMS1000 (Wetzlar, Germany). The scaffolds were imaged by scanning electron microscopy (SEM) and their cross-sections were observed by SEM and energy dispersive spectroscopy (SEM/EDS) on a FEI Nova 200 FEG-SEM/EDS (FEI Europe Company, Hillsboro, OR, USA). The microstructure of the scaffolds was analyzed by computed micro-tomography (micro-CT) using a high-resolution SkyScan 1272 scan (v1.1.3, Bruker, Boston, MA, USA). Samples were scanned using a pixel size of 21.6 μm , with a voltage of 60 kV and a current of 163 μA . The resulting images were reconstructed along the z-axis (software NRecon, SkyScan), then representative images were binarized through a global threshold (value adjusted to the minimum of the global grayscale histogram from each sample) (CTAn software, SkyScan). The reconstructed slice images were processed and through 3D rendering the mean pore size (μm), mean wall thickness (μm), and porosity (%) were determined. Finally, the 3D virtual reconstructions were created using the CTVox software (version 3.3.0 r1412, SkyScan, Boston, MA, USA). At least three samples were analyzed for each condition. Uniaxial compression tests of 3D-printed scaffolds were performed on a Instron 5969 (Norwood, MA, USA), equipped with a 50 kN load cell, setting the initial grip distance at 4 mm and the testing speed at 1 mm/s. At least five samples were analyzed for each condition. The samples were previously soaked overnight in a phosphate buffered saline (PBS) solution at 37 °C. Dynamical Mechanical Analysis (DMA) was performed using a TRITEC2000B equipment (Triton Technology, Grantham, UK) in compressive mode for the 3D-printed scaffolds and in tension mode for the braided scaffolds, with the aim of evaluating their mechanical properties and possible alterations when subjected to cyclic loading and immersed in physiologic fluids. Samples were previously soaked overnight in a PBS solution at 37 °C. DMA spectra were obtained at the same temperature using cycles of increasing frequency from 0.2 to 2 Hz. At least three samples were tested for each composition and scaffold type.

3. Results and Discussion

3.1. Scaffold Architecture and Morphology

The MFI results obtained for the composites reinforced with 0.5 and 2 wt.% of EG, f-EG and [(f-EG)+Ag] are summarized in Table S2, ranging from 10 to 14.5 g/10 min, which are adequate for use in extrusion-based processes. The addition of reinforcement did not significantly change the MFI measured for neat PLA. Scaffolds with a porous interconnected network and a pore size greater than 250 μm were produced, aiming at enabling ligament regeneration [25,33]. As expected, the production of 3D-printed scaffolds was faster, easier, and yielded reproducible samples.

During 3D printing optimization, accumulation of material, deformation of some layers, and/or closing of the pores, were defects observed and related to overheating. The scaffolds printed horizontally with nozzle temperature and printing velocity set at 185 °C and 45 $\text{mm}\cdot\text{s}^{-1}$, respectively, the build platform kept at 80 °C, an infill distance of 0.8 mm and layer height of 0.15 mm, and with a substrate of 5° contact angle exhibited well defined pores, with no deformation of layers, as well as no surface distortions. Therefore, these printing conditions were selected to produce all 3D-printed scaffolds. It is worth noting that horizontal printing required the deposition of a support layer. The same material of the scaffold was used, printing at a 5° contact angle (see Figure 1), which could be easily removed after cooling. Figure 3 presents the 3D-printed scaffolds of PLA and PLA reinforced with [(f-EG)+Ag]. A general view is provided in Figure 3a–c). The images obtained at higher magnification in the “front”, “top”, and “lateral” directions were

acquired as indicated in Figure 1. Further images of the 3D-printed scaffolds at all the compositions of EG, f-EG, and [(f-EG)+Ag] are presented in Figures S1–S4.

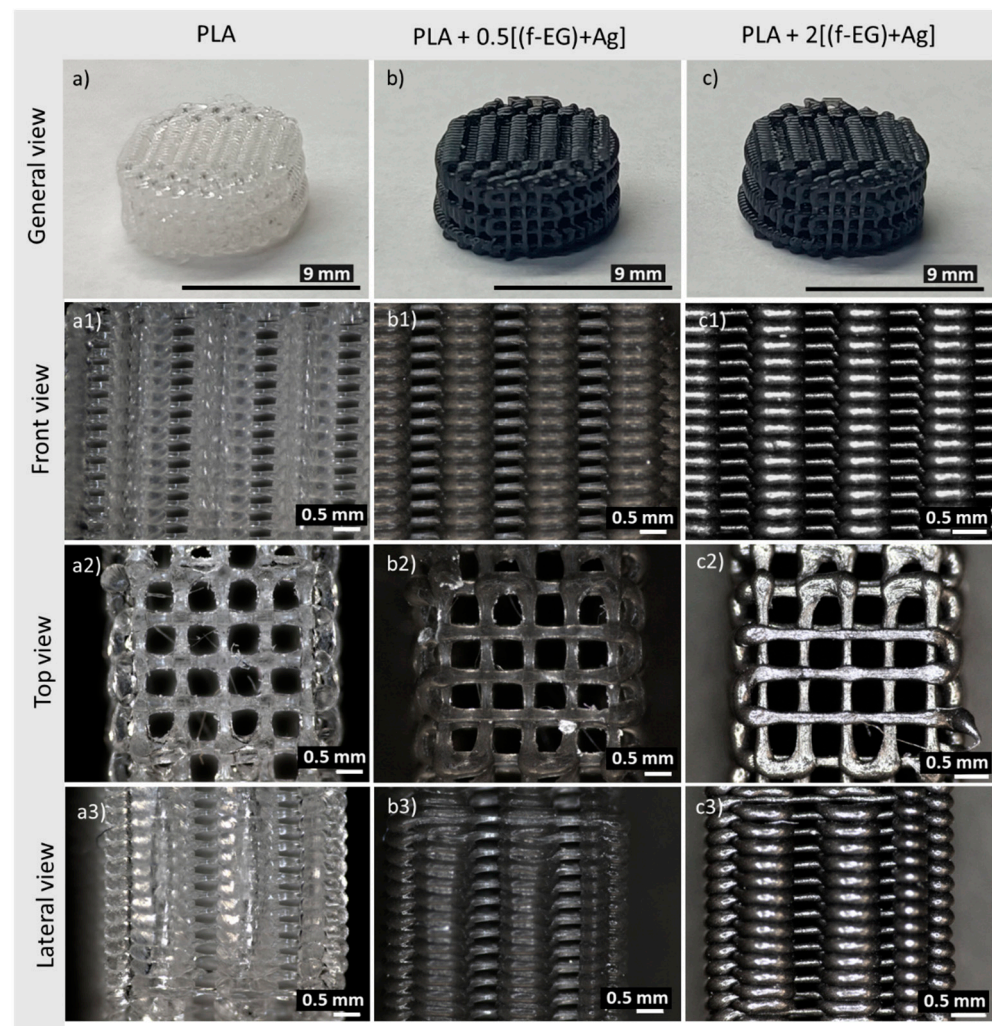


Figure 3. Three-dimensional-printed scaffolds: general view ((a)—PLA; (b)—PLA+0.5[(f-EG)+Ag]; (c)—PLA+2[(f-EG)+Ag]); higher magnification ((a1)–(a3)—PLA; (b1)–(b3)—PLA+0.5[(f-EG)+Ag] and (c1)–(c3)—PLA+2[(f-EG)+Ag]) from front, top, and side perspectives.

The general architecture of the braided scaffolds containing PLA and PLA reinforced with [(f-EG)+Ag] is illustrated in Figure 4a–c). The samples had a regular geometry, with large pores regularly distributed with clear pore interconnectivity.

The surface morphology of 3D-printed and braided scaffolds was observed by SEM (Figure 5). A slight roughness may be assigned to the presence of fillers, which may be advantageous for the application. It has been reported that surface roughness at micron and submicron scale may positively affect cell adhesion and proliferation regardless of the cell type and scaffold materials [33]. The braided scaffold geometry presents higher pore size compared to the 3D-printed scaffold. The addition of reinforcements did not significantly affect the scaffolds' geometry or pore size, either for braided or 3D-printed scaffolds.

The qualitative and quantitative analysis of porosity, mean pore size, and mean pore thickness of the 3D-printed and braided scaffolds were assessed by micro-CT and are summarized in Table 1. All 3D-printed scaffolds presented uniform pores over the entire surface and a similar structure, regardless of the presence of fillers, as illustrated in Figure 6 by the representative images of 3D-printed scaffolds containing PLA, PLA reinforced with 2 wt.% EG, (f-EG) and [(f-EG)+Ag]. Micro-CT cross-section images of the 3D-printed

scaffolds produced with the remaining compositions of EG, (f-EG) and [(f-EG)+Ag] are displayed in Figure S5.

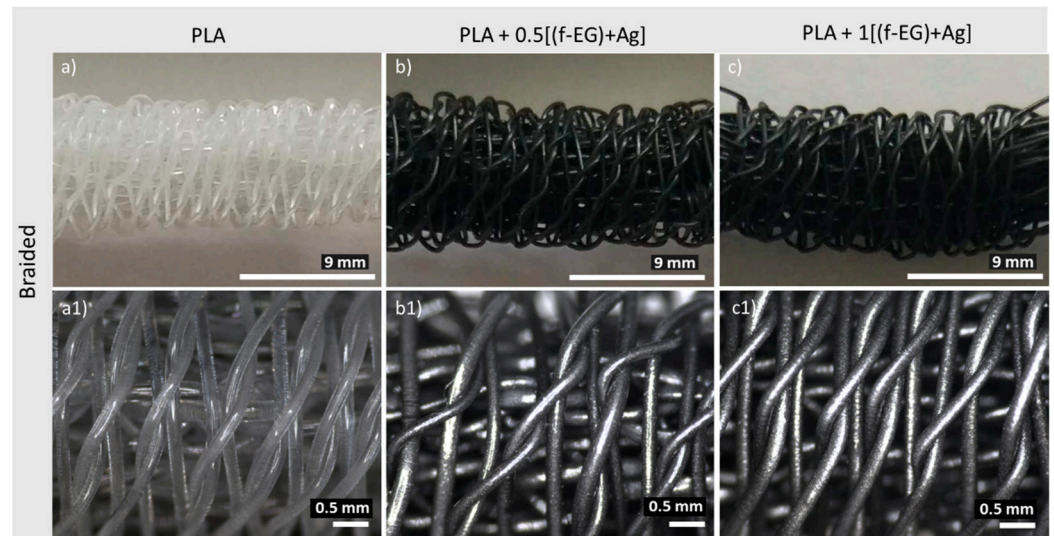


Figure 4. General view of braided scaffolds (longitudinal direction) containing: (a—PLA; b—PLA+0.5[(f-EG)+Ag]; c—PLA+1[(f-EG)+Ag]) and the corresponding optical images at higher magnification (a1–c1).

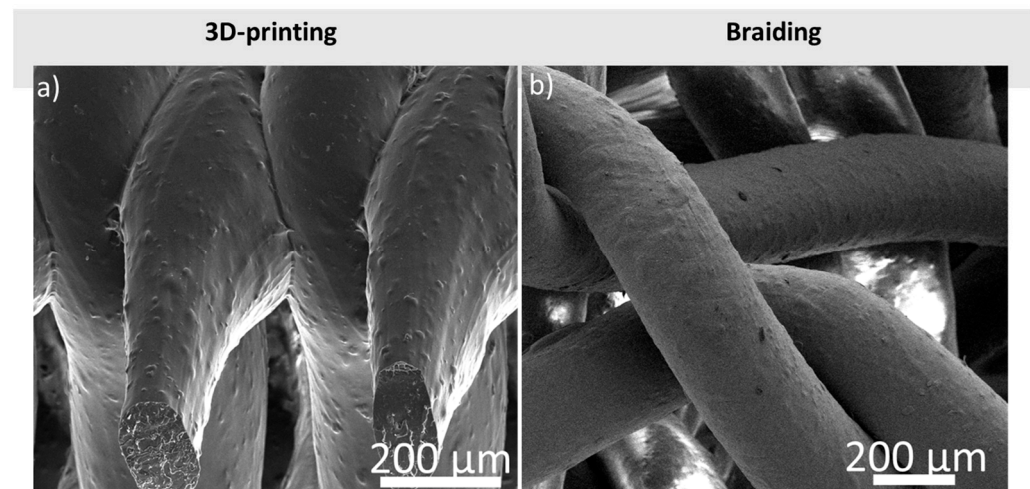


Figure 5. Morphology of the surface of the (a) 3D-printed scaffold containing PLA+2[(f-EG)+Ag], and (b) braided scaffold with PLA+1[(f-EG)+Ag].

Table 1. Mean porosity, pore size, and filament thickness of the 3D-printed and braided scaffolds, calculated from the micro-CT data.

Scaffold		Mean Porosity (%)	Mean Filament Thickness (μm)	Mean Pore Size (μm)
3D-printed	PLA	66.8 ± 1.5	240 ± 3	484 ± 4
	PLA+0.5 [(f-EG)+Ag]	70.5 ± 1.7	229 ± 8	496 ± 7
	PLA+2 [(f-EG)+Ag]	68.9 ± 0.8	236 ± 7	485 ± 17
Braided	PLA	87.6 ± 0.7	264 ± 34	1035 ± 411
	PLA+0.5 [(f-EG)+Ag]	83.4 ± 2.5	225 ± 33	1154 ± 8
	PLA+1 [(f-EG)+Ag]	87.8 ± 3.8	267 ± 33	1164 ± 545

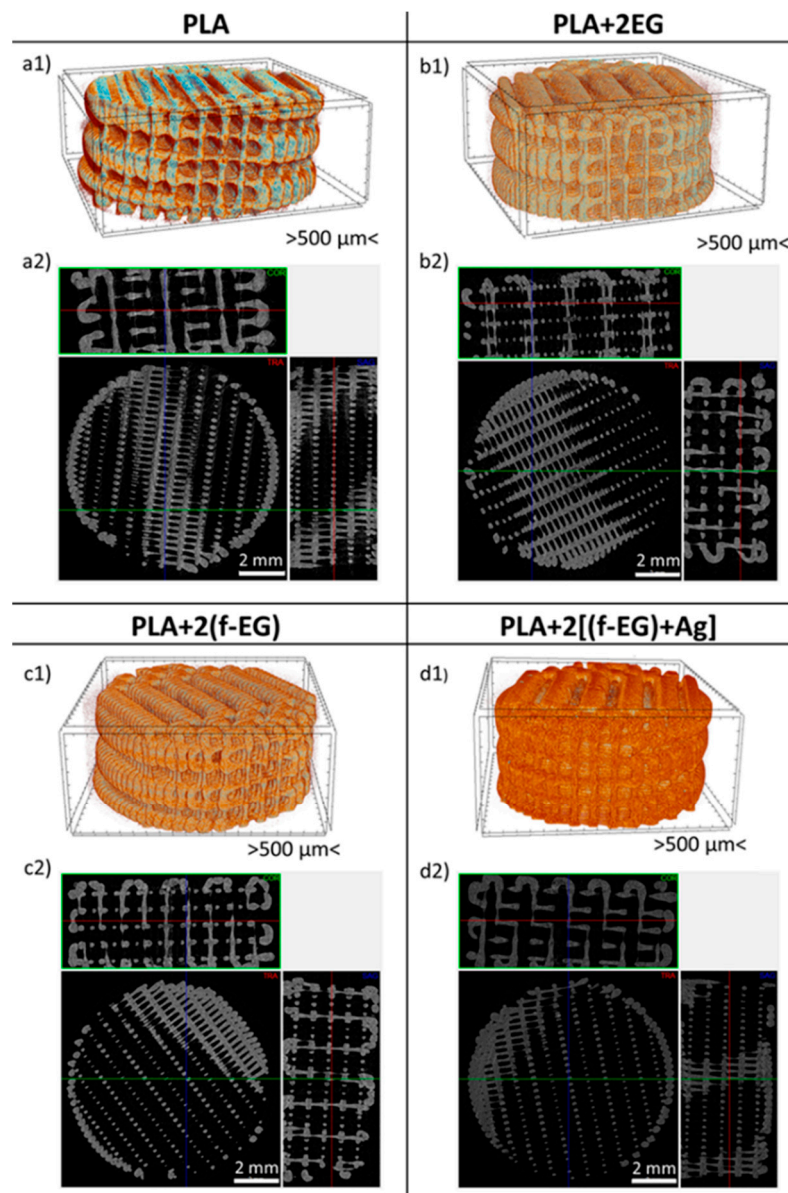


Figure 6. Representative 3D micro-CT reconstruction and the corresponding micro-CT cross-sections images of the 3D-printed scaffolds containing: (a1,a2) PLA; (b1,b2) PLA+2EG; (c1,c2) PLA+2(f-EG); and (d1,d2) PLA+2[(f-EG)+Ag].

PLA 3D-printed scaffolds exhibited a slightly lower porosity as compared to PLA+0.5[(f-EG)+Ag] and PLA+2[(f-EG)+Ag] 3D-printed scaffolds. Similar results were obtained for all 3D-printed scaffolds with different compositions (see Table S3), indicating that filler addition to the PLA matrix had a slight effect on pore morphology and size, during 3D printing, as reported by other authors [4].

Higher porosity and pore size were observed for braided scaffolds as compared to 3D-printed scaffolds. A large variation of the pore size was observed for the braided scaffolds, characteristic of the braiding design chosen and enhanced by the handcrafted production. The micro-CT images and 3D reconstructions are illustrated in Figure 7. Micro-CT analysis revealed similar porosity and pore size results for the braided scaffolds of PLA and composites with different compositions.

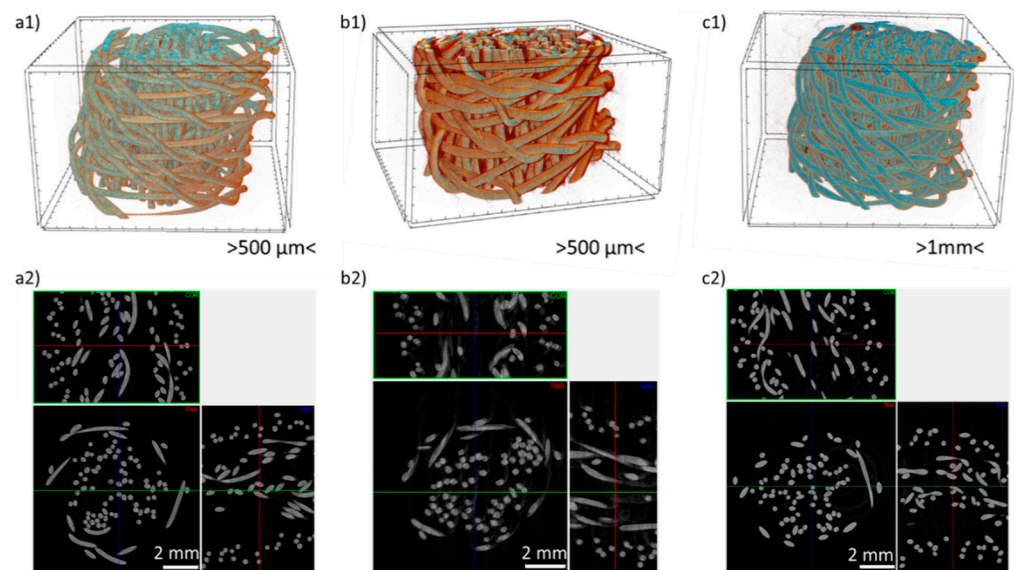


Figure 7. Representative 3D micro-CT reconstruction and micro-CT cross-sections images of the braided scaffolds containing (a1,a2) PLA, (b1,b2) PLA+0.5[(f-EG)+Ag], and (c1,c2) PLA+1[(f-EG)+Ag].

Pore interconnectivity and high porosity play an important role in the performance of scaffolds, helping the diffusion of nutrients, vascularization, and tissue ingrowth [34,35]. For ACL tissue engineering, it has been recognized that the scaffold should have an overall porosity >50% and exhibit pores with diameters greater than 250 μm [35,36]. Thus, the scaffolds produced in the present work, either 3D-printed or braided, exhibit adequate porosity, pore interconnectivity, and pore size for ACL regeneration. The pore size and morphology of 3D-printed scaffolds are comparable to those reported for other 3D-printed graphene-based scaffolds, such as PLA/GO [4] and polycaprolactone/reduced GO [37]. Braided scaffolds also exhibit a pore size similar to that found in other works focused on textile-based scaffolds for ligament regeneration such as knitted scaffolds of PLA/poly lactic-co-glycolic acid [38] and silk/collagen [39].

3.2. Morphology of the Nanoparticle Dispersion after 3D-Printing

The braiding process does not affect the nanoparticle dispersion morphology since the filaments produced by melt extrusion are only subjected to a textile process. However, 3D-Printing involves re-melting and flow, which may affect the dispersion state of the nanoparticles in the composite. In order to evaluate the nanoparticle dispersion morphology after 3D-printing, the scaffolds cross-sections were observed by SEM and compared to the morphology of the Fil3D used in the printing process. Figure 8 presents micrographs of the cross-sections of 3D-printed scaffolds containing PLA, PLA+0.5[(f-EG)+Ag], and PLA+2[(f-EG)+Ag] as well as of the Fil3D nanocomposite filaments that originated them.

Figure 8 illustrates the homogenous dispersion and distribution of [(f-EG)+Ag] in PLA for Fil3D filaments and its preservation after 3D-printing. Figure S6 depicts micrographs of the cross-sections of 3D-printed scaffolds produced with composite filaments containing 1 wt.% of EG, (f-EG) and [(f-EG)+Ag], showing similar morphology and good dispersion of the nanoparticles for all compositions.

The EDS elemental analysis of the 3D-printed scaffold containing PLA+2[(f-EG)+Ag] is depicted in Figure 9, confirming the presence of silver nanoparticles anchored on f-EG. The addition of silver nanoparticles onto graphene-based materials was reported to enhance the antimicrobial activity and biocompatibility, depending on its concentration [40,41]. The Au signal is due to the thin Au layer deposition performed to allow the SEM analysis.

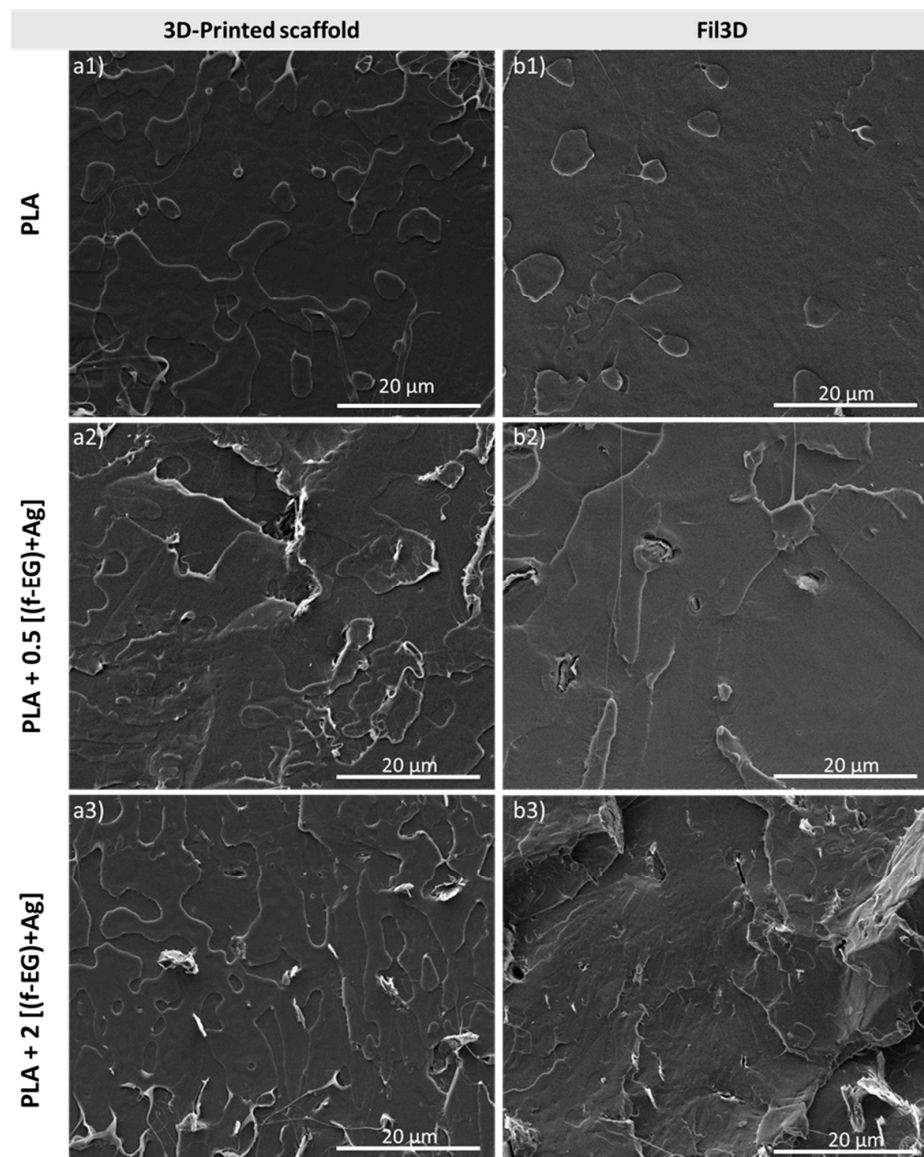


Figure 8. Morphology of the cross-section of the (a1–a3) 3D-printed filament scaffolds and (b1–b3) Fil3D containing PLA, PLA+0.5[(f-EG)+Ag], and PLA+2[(f-EG)+Ag], respectively.

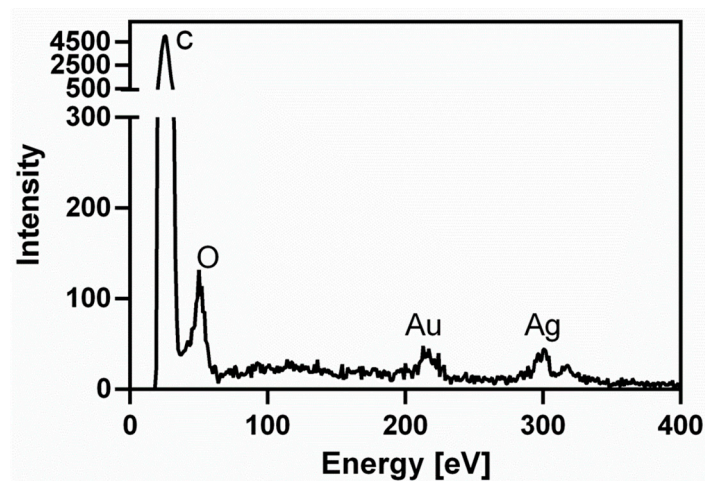


Figure 9. EDS of the 3D-printed scaffold containing PLA+2[(f-EG)+Ag].

3.3. Scaffold Dynamic Mechanical Analysis

The dynamic mechanical properties measured under wet conditions at 37 °C as a function of frequency are displayed in Figures 10 and 11, with Figure 10(a1–c1) and Figure 11(a1) representing the storage modulus (E') and Figure 10(a2–c2) and Figure 11(a2) the loss factor ($\tan \delta$) of 3D-printed and braided scaffolds, respectively.

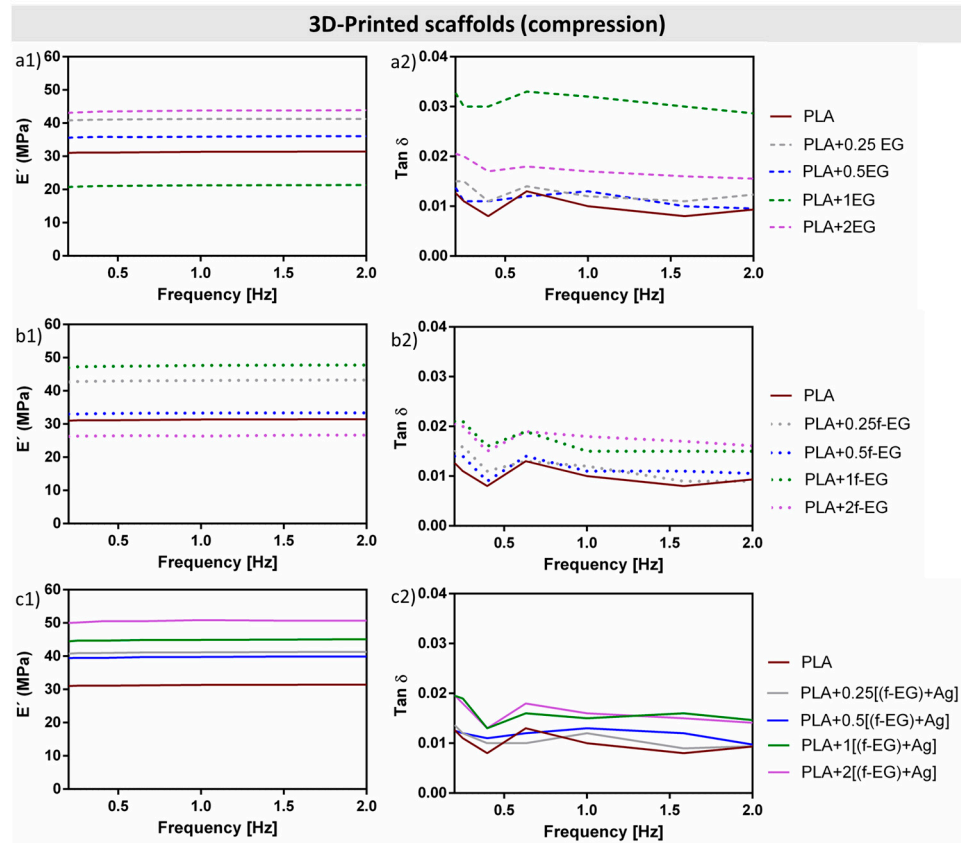


Figure 10. (a1–c1) Storage modulus (E') of 3D-printed scaffolds reinforced with EG, f-EG, and [(f-EG)+Ag], respectively, and (a2–c2) the corresponding loss factor ($\tan \delta$), as a function of the frequency, ranging from 0.1 to 2 Hz. Three-dimensional printed scaffolds were tested in compression mode.

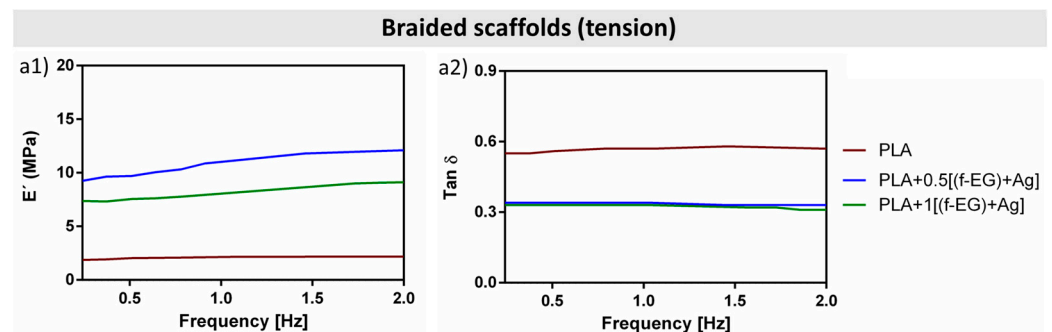


Figure 11. (a1) Storage modulus (E') and (a2) loss factor ($\tan \delta$) of braided scaffolds, as a function of the frequency, ranging from 0.1 to 2 Hz. Braided scaffolds were tested in tensile mode.

Several studies have reported the mechanical improvement of PLA reinforced with graphene-based materials under static loading [42]. The mechanical response of knee ligaments, namely ACL, posterior cruciate ligament (PCL), medial collateral ligament (MCL), and lateral collateral ligament (LCL) under static loading is also well documented [13,27]. Values reported for the elastic modulus of ACL, PCL, MCL, and LCL are in

the range of 65–447, 150–447, 330, and 245 MPa, respectively. Values reported for the ultimate strain are 14–44% for ACL, 11–19% for PCL, 17% for MCL, and 16% for LCL [27]. The ACL is formed by two anatomical bands (anteromedial (AMB) and posterolateral (PLB) bands). Tensile tests of porcine ACL bundles, similar to human ACL, showed that the stiffness of the PLB was significantly higher than that of the AMB, except for the modulus (111 and 123 MPa, respectively). In fact, no material property of intact ACL, AMB, and PLB specimens was significantly different, including deformation and strain at failure [43]. However, ligaments experience dynamic loads during normal locomotion, and their response is influenced by their viscoelastic properties. Thus, it is crucial to confirm the viscoelastic response of the scaffold structure to loading [42]. Studies reporting dynamic mechanical tests of PLA/graphene-based composite structures for ligament scaffolds are scarce [44–46]. Pinto et al. [44] produced composites for ACL regeneration based on CNTs functionalized with carboxylic acid (0.3 wt.%) by melt mixing/compression molding and observed an increase of 4% in the storage modulus compared to neat PLA, at 1 Hz and under tension. They also produced composites of PLA/GNPs (2 wt.%) by the same method and observed a decrease (2%) in the storage modulus relative to the neat polymer matrix.

The dynamic mechanical performance of 3D-printed and braided scaffolds may be affected not only by the scaffold's material but also by its structure. Thus, direct comparison of the DMA results obtained for 3D-printed and braided scaffolds is not appropriate. In general, an increase in E' is observed for the composite 3D-printed and braided scaffolds relative to PLA scaffolds, as presented in Figure 10(a1–c1) and Figure 11(a1), respectively. This is a consequence of the addition of high stiffness nanoparticles forming strong/rigid interfaces with the PLA matrix and reducing the polymer mobility near the nanofillers [47], or even to changes in the polymer crystallinity induced by the graphene nanoparticles. Graphene may act as a nucleating agent, restricting the movement of the polymer chains and inducing crystallization [42]. These effects may contribute differently to the 3D-printed and braided scaffolds since they were produced from filaments with different diameters and exhibiting distinct structures. Moreover, 3D-printing required re-melting of the filament to produce a continuous porous structure.

The DMA of 3D-printed scaffolds was conducted in compression mode, commonly used to mechanically characterize scaffolds obtained by 3D-printing [48,49]. The E' of 3D-printed scaffolds was nearly constant for the studied frequency range and, in general, increased with the addition of graphite nanoparticles, as compared to neat PLA, even with the addition of 0.25 wt.% of EG (as received and functionalized). The highest increase in the storage modulus at 37 °C and 1 Hz was observed for PLA+1f-EG and PLA+2[(f-EG)+Ag] exhibiting a storage modulus of 58.4 ± 7 and 61.7 ± 9 MPa, respectively, while the PLA 3D-printed scaffold presented $E' = 31.4 \pm 10$ MPa—Figure 12a), thus representing a 85% and 96% increase, respectively.

Braided scaffolds exhibit a fibrous and more complex geometry, similar to the hierarchical structure of the native ligament [27]. Their dynamic mechanical response was tested under tension, as commonly used for testing textile-based scaffolds [50]. Composite braided scaffolds possessed higher E' values compared to PLA braided scaffolds, which increased slightly with increasing frequency. An increase in the storage modulus was achieved at 37 °C and 1 Hz for scaffolds reinforced with 0.5 and 1 wt.% of [(f-EG)+Ag], reaching 11.1 ± 2 and 7.7 ± 2 MPa, respectively, compared to PLA (2.2 ± 2 MPa), see Figure 12b, representing a 400% and a 250% increase relative to PLA scaffolds, respectively.

The addition of micronized graphite/few-layer graphene to PLA at low concentrations by melt mixing was reported to produce composites with tensile properties that could be adequate for ligament regeneration applications, without significantly impairing the ductility [51]. Similar conclusions were obtained in the present work for compression tests performed on 3D-printed scaffolds about the effect of reinforcement on the composite ductility. The resulting compression stress–strain curves are shown in Figure S7(a1–c1). All scaffolds present an elastic region up to approximately 5% deformation, followed by a plateau region where their load-carrying capacity is maintained and plastic deformation

develops as well as structure yielding, followed by a densification region above 40% deformation, similarly to the results described by M. Saleh et al. [52]. Thus, from the point of view of ductility and compression strength, the compression test results indicate a similar performance of the 3D printed PLA and composite specimens.

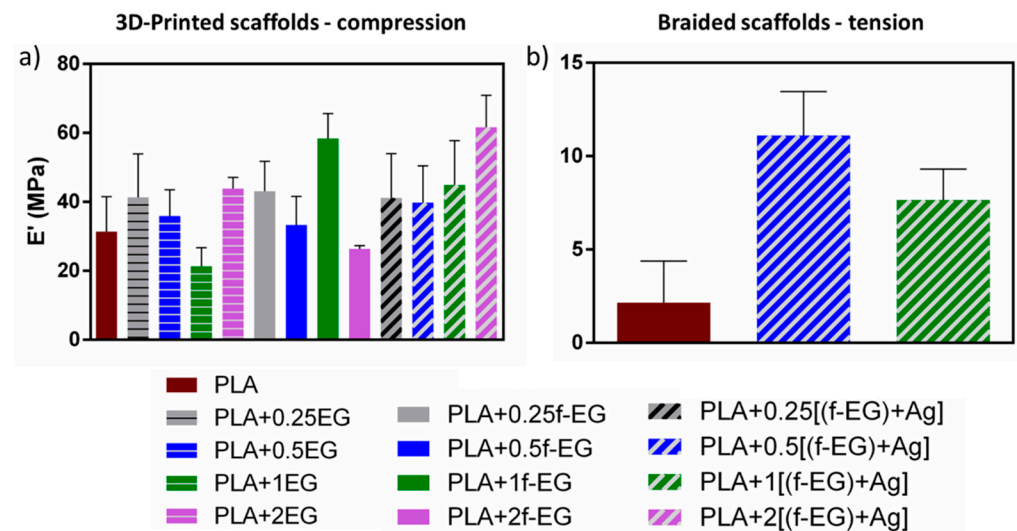


Figure 12. DMA results for the E' of (a) 3D-printed (under compression) and (b) braided scaffolds (under tension) at 37 °C and 1 Hz.

The viscoelastic nature of both 3D-printed and braided scaffolds was also confirmed by the loss factor values of DMA (Figures 10(a2–c2) and 11(a2)), ranging from 0.02–0.04 and 0.31–0.58, respectively), and suggest that both scaffolds have the capacity to dissipate energy and damping for the tested frequencies [53]. The incorporation of fillers also led to a decrease in the damping factor compared to PLA, which is a consequence of the reduced molecular mobility [54].

The storage modulus achieved for the 3D-printed scaffolds is in the same order of magnitude of the dynamic mechanical response reported for ligaments under compression at 1 Hz [55]. M. Najafidoust et al. [55] performed dynamic compression mechanical tests in ligaments in a wider range of frequencies (0.01–100 Hz) and at three different preloads (0.25, 0.75, and 2 N). An increase in the storage modulus was observed with increasing preload. At 1 Hz, all samples with different preloads exhibited a storage modulus ranging from approximately 4 to 21 MPa. Other studies measured the viscoelastic properties of ACL [56] and tendons [56,57] in tension mode, at body temperature and 1 Hz. For instance, J.H. Edwards et al. [57] suggested a xenogeneic tendon intended for ACL replacement and evaluated the dynamic mechanical response of a native and a decellularized tendon. At 1 Hz, the decellularized tendon exhibited a lower storage modulus than the native tendon, but in the same order of magnitude (MPa). The tan delta slightly decreased from 0 to approximately 0.7 Hz and was almost constant from 1 to 2 Hz. These results are similar to those found for the braided scaffolds.

4. Conclusions

Composite filaments based on PLA reinforced with EG, f-EG, and [(f-EG)+Ag] were successfully processed into three-dimensional scaffolds using textile-engineered and 3D-printing techniques. The production of 3D-printed scaffolds was faster, easier, and more reproducible compared to braided scaffolds, but all have finely controlled dimensions and geometry. Regardless of the filler, either EG, (f-EG) or [(f-EG)+Ag], a good dispersion and interaction with the polymeric matrix was observed through the cross section of 3D-printed scaffolds. The anchoring of a small concentration of Ag as an anti-microbial agent was confirmed by EDS on scaffolds reinforced with [(f-EG)+Ag]. The addition of

nanoparticles to the PLA matrix had a very slight effect on pore morphology and size. Three-dimensional-printed scaffolds exhibited a porosity that ranged from 67 to 71% and pore size from 484 to 496 μm . Higher porosity was observed for braided scaffolds compared to 3D-printed scaffolds, ranging from 83–88%, and pore size from 1035 to 1164 μm . Both braided and 3D-printed exhibited a viscoelastic behavior and an increase in the storage modulus for the composite scaffolds compared to neat PLA scaffolds. The highest E' was achieved by the scaffold containing PLA+2[(f-EG)+Ag] ($E' = 61.7 \pm 9$ MPa), among the 3D-printed scaffolds, and the scaffold with PLA+0.5 [(f-EG)+Ag] ($E' = 11.1 \pm 2$ MPa), among the braided scaffolds. Both braided and 3D-printed scaffolds exhibited storage modulus values comparable to those measured for ligaments/tendons in tension and compression, as well as high porosity and pore size adequate for ACL regeneration.

Supplementary Materials: The following supporting information can be downloaded at: <https://www.mdpi.com/article/10.3390/jcs7030104/s1>. Table S1: Thermogravimetric analysis of composite filaments and the percentage residual weight.; Table S2. MFI of filaments containing PLA and PLA reinforced with 0.5 and 2 wt.% of EG, f-EG and [(f-EG)+Ag].; Figure S1: Digital microscopy images of 3D-printed scaffolds containing (a1–a3—PLA+0.25EG; b1–b3—PLA+0.25(f-EG) and c1–c3—PLA+0.25[(f-EG)+Ag]) from a front, top, and side perspectives.; Figure S2: Digital microscopy images of 3D-printed scaffolds containing (a1–a3—PLA+0.5EG; b1–b3—PLA+0.5(f-EG) and c1–c3—PLA+0.5[(f-EG)+Ag]) from a front, top, and side perspectives.; Figure S3: Digital microscopy images of 3D-printed scaffolds containing (a1–a3—PLA+1EG; b1–b3—PLA+1(f-EG) and c1–c3—PLA+1[(f-EG)+Ag]) from a front, top, and side perspectives.; Figure S4: Digital microscopy images of 3D-printed scaffolds containing: a1–a3—PLA+2EG; b1–b3—PLA+2(f-EG) and c1–c3—PLA+2[(f-EG)+Ag], from a front, top, and side perspectives.; Figure S5: Representative micro-CT cross-sections images of the 3D-printed scaffolds containing PLA reinforced with 0.25, 0.5, 1 wt.% of EG, (f-EG) and [(f-EG)+Ag].; Table S3: Mean porosity, pore size, and filament thickness of 3D-printed scaffolds containing composites of EG, f-EG, and 0.25 and 1wt.% of [(f-EG)+Ag], calculated from the micro-CT data.; Figure S6: SEM images of 3D-printed scaffolds: a1—PLA+1EG; b—PLA+1(f-EG) and c—PLA+1 [(f-EG)+Ag].; Figure S7: Compressive test of 3D-printed scaffolds containing PLA and a1—EG, b1—f-EG and c1—[(f-EG)+Ag].

Author Contributions: M.S.—investigation; writing—original draft; formal analysis; N.M.A.—conceptualization; writing—review and editing; M.C.P.—conceptualization; writing—review and editing; I.P.—investigation; H.G.—investigation; A.C.V.—investigation; J.A.C.—conceptualization; writing—review and editing. All authors have read and agreed to the published version of the manuscript.

Funding: This research was funded by FCT through the National Funds Reference UIDB/05256/2020 and UIDP/05256/2020, the FCT and European Program FEDER/COMPETE through the project PTDC/BTM-MAT/28123/2017, and the FCT, European Union and European Social Fund (FSE) through the PhD Grant Reference SFRH/BD/138244/2018.

Data Availability Statement: Data is contained within this article and Supplementary Material.

Acknowledgments: IPC acknowledges the support of the Portuguese Foundation for Science and Technology (FCT) through the National Funds Reference UIDB/05256/2020 and UIDP/05256/2020. I3Bs acknowledges the support of FCT through the Project SeaJellyBone (PTDC/BTM-MAT/28123/2017). Silva M acknowledges FCT for the Grant Reference SFRH/BD/138244/2018 and is thankful to Alberto Campuzano for the support provided in the 3D printing process.

Conflicts of Interest: The authors declare no conflict of interest.

References

1. Altman, G.H.; Horan, R.L.; Lu, H.H.; Moreau, J.; Martin, I.; Richmond, J.C.; Kaplan, D.L. Silk matrix for tissue engineered anterior cruciate ligaments. *Biomaterials* **2002**, *23*, 4131–4141. [[CrossRef](#)]
2. Kuo, C.K.; Marturano, J.E.; Tuan, R.S. Novel strategies in tendon and ligament tissue engineering: Advanced biomaterials and regeneration motifs. *Sport. Med. Arthros. Rehab. Ther. Technol.* **2010**, *2*, 20. [[CrossRef](#)] [[PubMed](#)]
3. Ferrigno, B.; Bordett, R.; Duraisamy, N.; Moskow, J.; Arul, M.R.; Rudraiah, S.; Nukavarapu, S.P.; Vella, A.T.; Kumbar, S.G. Bioactive polymeric materials and electrical stimulation strategies for musculoskeletal tissue repair and regeneration. *Bioact. Mater.* **2020**, *5*, 468–485. [[CrossRef](#)] [[PubMed](#)]
4. Belaid, H.; Nagarajan, S.; Teyssier, C.; Barou, C.; Barés, J.; Balme, S.; Garay, H.; Huon, V.; Cornu, D.; Cavallès, V.; et al. Development of new biocompatible 3D printed graphene oxide-based scaffolds. *Mater. Sci. Eng. C* **2020**, *110*, 110595. [[CrossRef](#)] [[PubMed](#)]
5. Ge, Z.; Yang, F.; Goh, J.C.; Ramakrishna, S.; Lee, E.H. Biomaterials and scaffolds for ligament tissue engineering. *J. Biomed Mater. Res. A* **2006**, *77*, 639–652. [[CrossRef](#)]
6. Laurencin, C.T.; Freeman, J.W. Ligament tissue engineering: An evolutionary materials science approach. *Biomaterials* **2005**, *26*, 7530–7536. [[CrossRef](#)]
7. Lu, H.H.; Cooper, J.A.; Manuel, S.; Freeman, J.W.; Attawia, M.A.; Ko, F.K.; Laurencin, C.T. Anterior cruciate ligament regeneration using braided biodegradable scaffolds: In vitro optimization studies. *Biomaterials* **2005**, *26*, 4805–4816. [[CrossRef](#)]
8. Freeman, J.W.; Woods, M.D.; Laurencin, C.T. Tissue engineering of the anterior cruciate ligament using a braid-twist scaffold design. *J. Biomech.* **2007**, *40*, 2029–2036. [[CrossRef](#)]
9. da Silva, D.; Kaduri, M.; Poley, M.; Adir, O.; Krinsky, N.; Shainsky-Roitman, J.; Schroeder, A. Biocompatibility, biodegradation and excretion of polylactic acid (PLA) in medical implants and theranostic systems. *Chem. Eng. J.* **2018**, *340*, 9–14. [[CrossRef](#)]
10. Gonçalves, C.; Pinto, A.M.; Machado, A.V.; Moreira, J.A.; Gonçalves, I.C.; Magalhães, F.D. Biocompatible reinforcement of poly(Lactic acid) with graphene nanoplatelets. *Polym. Compos.* **2018**, *39*, E308–E320. [[CrossRef](#)]
11. Lawal, A.T. Graphene-based nano composites and their applications. A review. *Biosens. Bioelectron.* **2019**, *141*, 111384. [[CrossRef](#)]
12. Kim, I.-H.; Jeong, Y.G. Polylactide/exfoliated graphite nanocomposites with enhanced thermal stability, mechanical modulus, and electrical conductivity. *J. Polym. Sci. B Polym. Phys.* **2010**, *48*, 850–858. [[CrossRef](#)]
13. Paiva, M.C.; Simon, F.; Novais, R.M.; Ferreira, T.; Proença, M.F.; Xu, W.; Besenbacher, F. Controlled Functionalization of Carbon Nanotubes by a Solvent-free Multicomponent Approach. *ACS Nano* **2010**, *4*, 7379–7386. [[CrossRef](#)]
14. Novais, R.M.; Simon, F.; Pötschke, P.; Villmow, T.; Covas, J.A.; Paiva, M.C. Poly(lactic acid) Composites with Poly(lactic acid)-Modified Carbon Nanotubes. *J. Polym. Sci. Part A Polym. Chem.* **2013**, *51*, 3740–3750. [[CrossRef](#)]
15. Bellet, P.; Gasparotto, M.; Pressi, S.; Fortunato, A.; Scapin, G.; Mba, M.; Menna, E.; Filippini, F. Graphene-Based Scaffolds for Regenerative Medicine. *Nanomaterials* **2021**, *11*, 404. [[CrossRef](#)]
16. Caetano, G.F.; Wang, W.; Chiang, W.-H.; Cooper, G.; Diver, C.; Blaker, J.J.; Frade, M.A.C.; Bártolo, P. 3D-Printed Poly(ϵ -caprolactone)/Graphene Scaffolds Activated with P1-Latex Protein for Bone Regeneration. *3D Print. Addit. Manuf.* **2018**, *5*, 127–137. [[CrossRef](#)]
17. Godoy-Gallardo, M.; Eckhard, U.; Delgado, L.M.; de Roo Puente, Y.J.D.; Hoyos-Nogués, M.; Gil, F.J.; Perez, R.A. Antibacterial approaches in tissue engineering using metal ions and nanoparticles: From mechanisms to applications. *Bioact. Mater.* **2021**, *6*, 4470–4490. [[CrossRef](#)] [[PubMed](#)]
18. Rajzer, I.; Kurowska, A.; Jabłoński, A.; Kwiatkowski, R.; Piekarczyk, W.; Hajduga, M.B.; Kopeć, J.; Sidzina, M.; Menaszek, E. Scaffolds modified with graphene as future implants for nasal cartilage. *J. Mater. Sci.* **2020**, *55*, 4030–4042. [[CrossRef](#)]
19. Burduşel, A.C.; Gherasim, O.; Grumezescu, A.M.; Mogoantă, L.; Ficai, A.; Andronesco, E. Biomedical Applications of Silver Nanoparticles: An Up-to-Date Overview. *Nanomaterials* **2018**, *8*, 681. [[CrossRef](#)]
20. Parchi, P.D.; Vittorio, O.; Andreani, L.; Battistini, P.; Piolanti, N.; Marchetti, S.; Poggetti, A.; Lisanti, M. Nanoparticles for Tendon Healing and Regeneration: Literature Review. *Front. Aging Neurosci.* **2016**, *8*, 202. [[CrossRef](#)] [[PubMed](#)]
21. Buckthorpe, M.; La Rosa, G.; Villa, F.D. Restoring knee extensor strength after anterior cruciate ligament reconstruction: A clinical commentary. *Int. J. Sport. Phys. Ther.* **2019**, *14*, 159–172. [[CrossRef](#)]
22. Imoto, A.M.; Peccin, S.; Almeida, G.J.; Saconato, H.; Atallah, Á.N. Effectiveness of electrical stimulation on rehabilitation after ligament and meniscal injuries: A systematic review. *Sao Paulo Med. J.* **2011**, *129*, 414–423. [[CrossRef](#)] [[PubMed](#)]
23. Yadegari-Dehkordi, S.; Sadeghi, H.R.; Attaran-Kakhki, N.; Shokouhi, M.; Sazgarnia, A. Silver nanoparticles increase cytotoxicity induced by intermediate frequency low voltages. *Electromagn. Biol. Med.* **2015**, *34*, 317–321. [[CrossRef](#)] [[PubMed](#)]
24. Silva, M.; Gomes, C.; Pinho, I.; Gonçalves, H.; Vale, A.C.; Covas, J.A.; Alves, N.M.; Paiva, M.C. Poly(Lactic Acid)/Graphite Nanoplatelet Nanocomposite Filaments for Ligament Scaffolds. *Nanomaterials* **2021**, *11*, 2796. [[CrossRef](#)]
25. Silva, M.; Ribeiro, D.; Cunha, E.; Proença, M.F.; Young, R.J.; Paiva, M.C. A Simple Method for Anchoring Silver and Copper Nanoparticles on Single Wall Carbon Nanotubes. *Nanomaterials* **2019**, *9*, 1416. [[CrossRef](#)] [[PubMed](#)]
26. Oluwadamilola, A.; Yousaf, S.; Zare, M.; Mozafari, M.; Youseffi, M.; Twigg, P.; Sefat, F. Scaffolds for ligament tissue engineering. In *Handbook of Tissue Engineering Scaffolds*, 1st ed.; Mozafari, M., Sefat, F., Atala, A., Eds.; Woodhead Publishing Series in Biomaterials: Amsterdam, The Netherlands, 2019; Volume 1, pp. 299–327.

27. Santos, M.L.; Rodrigues, M.T.; Domingues, R.M.A.; Reis, R.L.; Gomes, M.E. Biomaterials as Tendon and Ligament Substitutes: Current Development. In *Regenerative Strategies for the Treatment of Knee Joint Disabilities*, 1st ed.; Oliveira, J.M., Reis, R.L., Eds.; Springer: Cham, Switzerland, 2017; Volume 21, pp. 349–371.
28. Liu, H.; Fan, H.; Wang, Y.; Toh, S.L.; Goh, J.C. The interaction between a combined knitted silk scaffold and microporous silk sponge with human mesenchymal stem cells for ligament tissue engineering. *Biomaterials* **2008**, *29*, 662–674. [[CrossRef](#)]
29. Akbari, M.; Tamayol, A.; Bagherifard, S.; Serex, L.; Mostafalu, P.; Faramarzi, N.; Mohammadi, M.H.; Khademhosseini, A. Textile Technologies and Tissue Engineering: A Path Toward Organ Weaving. *Adv. Healthc. Mater.* **2016**, *5*, 751–766. [[CrossRef](#)]
30. Chung, J.J.; Im, H.; Kim, S.H.; Park, J.W.; Jung, Y. Toward Biomimetic Scaffolds for Tissue Engineering: 3D Printing Techniques in Regenerative Medicine. *Front. Bioeng. Biotechnol.* **2020**, *8*, 586406. [[CrossRef](#)]
31. An, J.; Teoh, J.E.M.; Suntornnond, R.; Chua, C.K. Design and 3D Printing of Scaffolds and Tissues. *Engineering* **2015**, *1*, 261–268. [[CrossRef](#)]
32. Ghilan, A.; Chiriac, A.P.; Nita, L.E.; Rusu, A.G.; Neamtu, I.; Chiriac, V.M. Trends in 3D Printing Processes for Biomedical Field: Opportunities and Challenges. *J. Polym. Environ.* **2020**, *28*, 1345–1367. [[CrossRef](#)]
33. Cai, S.; Wu, C.; Yang, W.; Liang, W.; Yu, H.; Liu, L. Recent advance in surface modification for regulating cell adhesion and behaviors. *Nanotechnol. Rev.* **2020**, *9*, 971–989. [[CrossRef](#)]
34. Cengiz, I.F.; Oliveira, J.M.; Reis, R.L. A Digital 3D Microstructural Voyage into Scaffolds: A Systematic Review of the Reported Methods and Results. *Biomater. Res.* **2018**, *22*, 26. [[CrossRef](#)]
35. Laurent, C.; Liu, X.; De Isla, N.; Wang, X.; Rahouadj, R. Defining a scaffold for ligament tissue engineering: What has been done, and what still needs to be done. *J. Cell. Immunother.* **2018**, *4*, 4–9. [[CrossRef](#)]
36. Mengsteab, P.Y.; Nair, L.S.; Laurencin, C.T. The past, present and future of ligament regenerative engineering. *Regen. Med.* **2016**, *11*, 871–881. [[CrossRef](#)]
37. Seyedsalehi, A.; Daneshmandi, L.; Barajaa, M.; Riordan, J.; Laurencin, C.T. Fabrication and characterization of mechanically competent 3D printed polycaprolactone-reduced graphene oxide scaffolds. *Sci. Rep.* **2020**, *10*, 22210. [[CrossRef](#)]
38. Ge, Z.; Goh, J.C.; Wang, L.; Tan, E.P.; Lee, E.H. Characterization of knitted polymeric scaffolds for potential use in ligament tissue engineering. *J. Biomater. Sci. Polym. Ed.* **2005**, *16*, 1179–1192. [[CrossRef](#)] [[PubMed](#)]
39. Chen, X.; Qi, Y.Y.; Wang, L.L.; Yin, Z.; Yin, G.L.; Zou, X.H.; Ouyang, H.W. Ligament regeneration using a knitted silk scaffold combined with collagen matrix. *Biomaterials* **2008**, *29*, 3683–3692. [[CrossRef](#)]
40. Khalil, W.A.; Sherif, H.H.A.; Hemdan, B.A.; Khalil, S.K.H.; Hotaby, W.E. Biocompatibility enhancement of graphene oxide-silver nanocomposite by functionalisation with polyvinylpyrrolidone. *IET Nanobiotechnol.* **2019**, *13*, 816–823. [[CrossRef](#)]
41. De Faria, A.F.; Martinez, D.S.T.; Meira, S.M.M.; de Moraes, A.C.M.; Brandelli, A.; Filho, A.G.S.; Alves, O.L. Anti-adhesion and antibacterial activity of silver nanoparticles supported on graphene oxide sheets. *Colloids Surf. B Biointerfaces* **2014**, *113*, 115–124. [[CrossRef](#)]
42. Peixoto, T.; Paiva, M.C.; Marques, A.T.; Lopes, M.A. Potential of Graphene–Polymer Composites for Ligament and Tendon Repair: A Review. *Adv. Eng. Mater.* **2020**, *22*, 2000492. [[CrossRef](#)]
43. Zhou, T.; Grimshaw, P.N.; Jones, C. A biomechanical investigation of the anteromedial and posterolateral bands of the porcine anterior cruciate ligament. *Proc. Inst. Mech. Eng. H* **2009**, *223*, 767–775. [[CrossRef](#)] [[PubMed](#)]
44. Pinto, V. Biodegradable Polymer Nanocomposites Reinforced with Carbon Nanostructures, PLA/CNT-COOH and PLA/GNP, for Augmentation Ligament Devices: Production and Characterization. Ph.D. Thesis, Faculdade de Engenharia da Universidade do Porto, Porto, Portugal, 2016.
45. Murariu, M.; Dechief, A.L.; Bonnaud, L.; Paint, Y.; Gallos, A.; Fontaine, G.; Bourbigot, S.; Dubois, P. The production and properties of polylactide composites filled with expanded graphite. *Polym. Degrad. Stab.* **2010**, *95*, 889–900. [[CrossRef](#)]
46. Cao, Y.; Feng, J.; Wu, P. Preparation of organically dispersible graphene nanosheet powders through a lyophilization method and their poly(lactic acid) composites. *Carbon* **2010**, *48*, 3834–3839. [[CrossRef](#)]
47. Li, X.; Xiao, Y.; Bergeret, A.; Longerey, M.; Che, J. Preparation of polylactide/graphene composites from liquid-phase exfoliated graphite sheets. *Polym. Compos.* **2014**, *35*, 396–403. [[CrossRef](#)]
48. Sharma, A.; Gupta, S.; Sampathkumar, T.S.; Verma, R.S. Modified graphene oxide nanoplates reinforced 3D printed multifunctional scaffold for bone tissue engineering. *Biomater. Adv.* **2022**, *134*, 112587. [[CrossRef](#)] [[PubMed](#)]
49. Gunes, O.C.; Kara, A.; Baysan, G.; Husemoglu, R.B.; Akokay, P.; Albayrak, A.Z.; Ergur, B.C.; Havitcioglu, H. Fabrication of 3D Printed poly(lactic acid) strut and wet-electrospun cellulose nano fiber reinforced chitosan-collagen hydrogel composite scaffolds for meniscus tissue engineering. *J. Biomater. Appl.* **2022**, *37*, 683–697. [[CrossRef](#)]
50. Almeida, L.R.; Martins, A.R.; Fernandes, E.M.; Oliveira, M.B.; Corrello, V.M.; Pashkuleva, I.; Marques, A.P.; Ribeiro, A.S.; Durães, N.F.; Silva, C.J.; et al. New biotextiles for tissue engineering: Development, characterization and in vitro cellular viability. *Acta Biomater.* **2013**, *9*, 8167–8181. [[CrossRef](#)]
51. Peixoto, T.; Nunes, J.; Lopes, M.A.; Marinho, E.; Proença, M.F.; Lopes, P.E.; Paiva, M.C. Poly(lactic acid) composites with few layer graphene produced by noncovalent chemistry. *Polym. Compos.* **2022**, *43*, 8409–8425. [[CrossRef](#)]
52. Saleh, M.; Anwar, S.; Al-Ahmari, A.M.; Alfaiy, A. Compression Performance and Failure Analysis of 3D-Printed Carbon Fiber/PLA Composite TPMS Lattice Structures. *Polymers* **2022**, *14*, 4595. [[CrossRef](#)]
53. Shearer, T.; Parnell, W.J.; Lynch, B.; Screen, H.R.C.; Abrahams, D.A. Recruitment Model of Tendon Viscoelasticity That Incorporates Fibril Creep and Explains Strain-Dependent Relaxation. *ASME J. Biomech. Eng.* **2020**, *142*, 071003. [[CrossRef](#)]

54. Costa, U.O.; Nascimento, L.F.C.; Almeida Bezerra, W.B.; de Oliveira Aguiar, V.; Pereira, A.C.; Monteiro, S.N.; Pinheiro, W.A. Dynamic Mechanical Behavior of Graphene Oxide Functionalized Curaua Fiber-Reinforced Epoxy Composites: A Brief Report. *Polymers* **2021**, *13*, 1897. [[CrossRef](#)] [[PubMed](#)]
55. Najafidoust, M.; Hashemi, A.; Oskui, I.Z. Dynamic viscoelastic behavior of bovine periodontal ligament in compression. *J. Periodont. Res.* **2020**, *55*, 651–659. [[CrossRef](#)]
56. Netti, P.; D'Amore, A.; Ronca, D.; Ambrosio, L.; Nicolais, L. Structure-mechanical properties relationship of natural tendons and ligaments. *J. Mater. Sci. Mater. Med.* **1996**, *7*, 525–530. [[CrossRef](#)]
57. Edwards, J.H.; Ingham, E.; Herbert, A. Decellularisation affects the strain rate dependent and dynamic mechanical properties of a xenogeneic tendon intended for anterior cruciate ligament replacement. *J. Mech. Behav. Biomed Mater.* **2019**, *91*, 18–23. [[CrossRef](#)] [[PubMed](#)]

Disclaimer/Publisher's Note: The statements, opinions and data contained in all publications are solely those of the individual author(s) and contributor(s) and not of MDPI and/or the editor(s). MDPI and/or the editor(s) disclaim responsibility for any injury to people or property resulting from any ideas, methods, instructions or products referred to in the content.